

PACS numbers: 52.40.Nk; 42.65.Sf; 42.65.Tg
DOI: 10.1070/QE2000v030n11ABEH001850

The specific features of self-action of high-power laser radiation propagating through a fully ionised cold plasma and the development of modulation instability

V A Aleshkevich, V A Vysloukh, Ya V Kartashov

Abstract. The features of the propagation of soliton-like light beams through a fully ionised two-dimensional cold plasma are considered employing analytical and numerical methods commonly used in nonlinear optics. Exact soliton profiles for the lower and upper soliton branches are found numerically in the presence of optical bistability. It is shown that the interaction of incoherent soliton-like laser beams in such a plasma may result both in the destruction of one of the beams and in production of new ones. The regime of the modulation instability of a plane wave propagating through a cold laser-produced plasma is studied.

1. Introduction

The interaction of high-power laser radiation with a plasma is among the branches of plasma physics that have been studied most actively in the past decade. This interaction is accompanied by a variety of processes, such as the relativistic self-trapping of a laser beam [1 – 3], excitation of coherent radiation at frequencies that are multiples to the plasma frequency [4], excitation of high-amplitude plasma waves [5, 6], the shift of the incident-radiation frequency induced by the plasma wave, particle acceleration [7], fast-electron production [8 – 11], etc. The rate of these processes increases significantly in the relativistic case, when the incident radiation intensity is so high that the velocity of electron quiver in the radiation field is comparable with the velocity of light.

In the general case, the study of collective processes in the plasma–light field system under study requires the use of numerical multiparticle techniques of the 3D PIC type [12, 13] or consideration of the infinite system of Bogolyubov chains for the multiparticle distribution function. Nevertheless, under specific conditions a plasma can be treated as a nonlinear medium with the refractive index that depends on the intensity of incident radiation. The nonlinear refractive index, in particular, can be introduced when employing a hydrodynamic plasma model in the quasi-static approximation [14, 15], when the plasma liquid in the coordinate system moving at the velocity of light finds itself in the field of quasi-stationary radiation with a slowly varying intensity. The implementation of this approach permits applying the analytical and numerical methods of nonlinear optics to the analysis of propagation of high-power laser radiation through plasmas.

In this paper, we investigate the principal features of the self-action of high-power light radiation during its propagation through a fully ionised cold laser-produced plasma and the development of modulation instability. The study is made on the basis of a truncated wave equation and the known expression for the nonlinear addition to the refractive index [16].

V A Aleshkevich, V A Vysloukh, Ya V Kartashov Department of Physics, M V Lomonosov Moscow State University, Vorob'evy gory, 119899 Moscow, Russia; tel.: (095) 939 34 38; fax: (095) 939 14 89; e-mail: azesh@gateway.phys.msu.su

Received 31 March 2000
Kvantovaya Elektronika **30** (11) 991 – 996 (2000)
Translated by E N Ragozin

2. Theoretical model

To describe the self-action of high-power laser radiation propagating along the z-axis in a fully ionised two-dimensional (with one transverse coordinate x) cold laser-produced plasma, we employ a dimensionless scalar potential $\phi(x, z, t) = e\Phi(x, z, t)/(2^{1/2}m_0c^2)$ and a dimensionless transverse vector potential $\boldsymbol{a}(x, z, t) = e\boldsymbol{A}_\perp(x, z, t)/(2^{1/2}m_0c^2)$ written using the Coulomb gauge $\nabla\boldsymbol{A}(x, z, t) = 0$ [16, 17] (the gauge implies that the longitudinal z-component of the vector potential is $A_z = 0$). Such is the case, e.g., when the laser plasma is produced with a cylindrical lens.

The theoretical model used below involves simultaneous solution of a conventional truncated wave equation

$$i\frac{\partial \boldsymbol{a}_s}{\partial z} = -\frac{1}{2k}\frac{\partial^2 \boldsymbol{a}_s}{\partial x^2} - k\frac{\delta n_{NL}}{n}\boldsymbol{a}_s \qquad (1)$$

for the intensity envelope of the perturbing electromagnetic field $\boldsymbol{a}_s(x, z, t) = \boldsymbol{a}(x, z, t)/\exp(ikz - i\omega t)$ slowly varying in z and t (where $k = \omega/c$ is the wave number, ω is the central frequency, and δn_{NL} is the nonlinear addition to the unperturbed refractive index n) and a set of constitutive equations in the form of relativistic hydrodynamic equations for a cold liquid (in which the thermal effects are disregarded), which describe approximately inherently nonlinear response of the plasma.

The following assumptions were made in the analysis of the obtained closed system of nonlinear equations [16]: (i) the polarisation of the incident radiation is arbitrary; (ii) the ions remain immobile because their mass is large compared to the electron mass; (iii) the radiation pulse duration τ greatly exceeds the characteristic plasma time $\tau_p = 1/\omega_p$ (where $\omega_p = (4\pi n_e e^2/m_0)^{1/2}$ is the characteristic plasma frequency, $n_e(x, z, t)$ is the average electron density in the plasma, and m_0 is the electron rest mass); (iv) the central frequency ω of the incident radiation considerably

exceeds the plasma frequency ω_p; (v) the characteristic transverse dimension of the light beam is $x_0 \gg c/\omega_p$; and (vi), the pulse duration is $\tau \gg x_0/c$, allowing us to neglect the dispersion effects compared to the diffraction ones.

Under the above assumptions, the following expression for the nonlinear addition to the refractive index of the plasma can be obtained from the hydrodynamic equations [16, 18]:

$$\delta n_{NL} = \frac{1}{2}\frac{\omega_p^2}{\omega^2}\frac{\left(1+|\boldsymbol{a}_s|^2\right)^{1/2}-1}{\left(1+|\boldsymbol{a}_s|^2\right)^{1/2}}. \tag{2}$$

In the limit of weak electromagnetic fields, the plasma behaves like a Kerr medium with a cubic nonlinearity. As the field intensity increases, the nonlinear response exhibits saturation. After substitution of expression (2) in the truncated wave equation, we eventually obtain that the radiation propagation is described by the following equation (the nonlinear Schrödinger equation):

$$\mathrm{i}\frac{\partial \boldsymbol{a}_s}{\partial \xi} = -\frac{1}{2}\frac{\partial^2 \boldsymbol{a}_s}{\partial \eta^2} - S\boldsymbol{a}_s\frac{\left(1+|\boldsymbol{a}_s|^2\right)^{1/2}-1}{\left(1+|\boldsymbol{a}_s|^2\right)^{1/2}}, \tag{3}$$

where $\eta = x/x_0$ is the normalised transverse coordinate; x_0 is the characteristic transverse scale of the beam; $\xi = z/L_d$ is the normalised longitudinal coordinate; $L_d = kx_0^2$ is the diffraction length corresponding to x_0; $S = L_d/L_{NL}$ is a parameter that determines the relative contributions of self-action and diffraction spreading; $L_{NL} = 2n\omega^2/(k\omega_p^2)$ is the characteristic nonlinear length; and $n = 1 - 0.5(\omega_p/\omega)^2$ is the unperturbed refractive index.

The characteristic transverse scale x_0 of the beam introduced in Eqn (3) is conveniently identified with the beam width determined at the level of half the light field intensity at the centre of the beam. This scaling results in the condition $\boldsymbol{a}_s(\xi = 0,\ \eta = 1) = 2^{-1/2}\boldsymbol{a}_s(\xi = 0, \eta = 0)$, which will be frequently used to find the profiles of soliton-like solutions for the lower and upper soliton branches. It is evident from Eqn (3) that the nonlinear plasma medium acts as a focusing lens in our case. A stable balance between the diffraction spreading and the nonlinear focusing is possible in such a focusing medium, which may result in a soliton-like beam propagation mode.

3. Profiles of soliton-like beams and their interaction

We will seek the stationary spatially localised solutions of Eqn (3) that describe soliton-like beams travelling at considerable distances without significant distortions of the initial profile. Because of saturation of the nonlinear response of the plasma, the profiles of soliton-like beams cannot be obtained analytically for arbitrary values of the parameter S and a numerical integration is required. Nevertheless, in the limiting case of low amplitudes of the normalised vector potential $\boldsymbol{a}_s$, we can find an approximate analytic solution because in this case Eqn (3) transforms to the nonlinear Schrödinger equation, which describes the propagation of solitons in Kerr media:

$$\mathrm{i}\frac{\partial \boldsymbol{a}_s}{\partial \xi} = -\frac{1}{2}\frac{\partial^2 \boldsymbol{a}_s}{\partial \eta^2} - \frac{1}{2}S\boldsymbol{a}_s|\boldsymbol{a}_s|^2. \tag{4}$$

The solution of Eqn (4) represents a well-known bright soliton which is described by the hyperbolic secant:

$$\boldsymbol{a}_s(\eta,\xi) = 2(b/S)^{1/2}\boldsymbol{e}\,\mathrm{sech}\left[(2b)^{1/2}\eta\right]\exp(\mathrm{i}b\xi), \tag{5}$$

where b is the propagation constant and $\boldsymbol{e}$ is the unit polarisation vector of the incident radiation. It is evident from expression (5) that passing to the Kerr nonlinear response model is justified for large parameter values $S \gg 1$ or, more precisely, for $b/S \ll 1$.

To determine the profiles of soliton-like beams for arbitrary values of the parameter S, we will use the iterative technique [19, 20]. In accordance with this technique, we will seek the stationary spatially limited solutions of Eqn (3) in the form

$$\boldsymbol{a}_s(\eta,\xi) = \boldsymbol{e}\rho(\eta)\exp(\mathrm{i}b\xi), \tag{6}$$

where $\rho(\eta)$ is a real function describing the soliton envelope. By substituting this expression in the truncated wave equation (3), we obtain the following second-order differential equation for the soliton envelope:

$$\frac{\mathrm{d}^2\rho}{\mathrm{d}\eta^2} = 2b\rho - 2S\rho\left[1 - \frac{1}{\left(1+\rho^2\right)^{1/2}}\right]. \tag{7}$$

Eqn (7) can be integrated once and reduced to the first-order equation for the envelope $\rho(\eta)$:

$$\frac{\mathrm{d}\rho}{\mathrm{d}\eta} = \left\{2b\rho^2 - 2S\rho^2 + 4S\left[\left(1+\rho^2\right)^{1/2}-1\right]\right\}^{1/2}. \tag{8}$$

Because of the saturation of the nonlinear response, the right-hand side of the equation obtained does not permit one more integration, which could yield an implicit dependence of the envelope ρ on the transverse coordinate η. For numerical integration, it is convenient to transform the differential equation (8) into the integral equation

$$\rho(\eta) = \rho_0\exp\left\{-2S^{1/2}\int_0^\eta\left[\frac{\left[1+\rho^2(\zeta)\right]^{1/2}-1}{\rho^2(\zeta)} - \frac{\left(1+\rho_0^2\right)^{1/2}-1}{\rho_0^2}\right]^{1/2}\mathrm{d}\zeta\right\}. \tag{9}$$

It has been taken into account in Eqn (9) that the propagation constant b can be uniquely determined using Eqn (8) taking into account that $\mathrm{d}\rho/\mathrm{d}\eta|_{\eta=0} = 0$:

$$b = S - 2S\left[\frac{\left(1+\rho_0^2\right)^{1/2}-1}{\rho_0^2}\right]. \tag{10}$$

Here, $\rho_0 = \rho(\eta = 0)$ is the amplitude of a spatially localised soliton solution. The numerical solution of the integral equation (9) can be obtained employing an iterative procedure. When performing integration, we set the function $\rho^{(0)}(\eta) = \rho_0\mathrm{sech}\,\eta$ as the initial one and took into account the above-mentioned requirement that $\rho(\eta = 1) = 2^{-1/2}\rho_0$, which follows from the normalisation of the transverse coordinate x. The iterative procedure quite rapidly converges to the precise soliton solution if the selected soliton amplitude ρ_0 corresponds to a given S.

Fig. 1a shows the amplitude ρ_0 of the soliton solution as a function of the parameter S. One can see that no localised soliton solutions exist for $S < S_{cr} \approx 1.8$. For $S > S_{cr}$ (the corresponding soliton amplitude is $\rho_0(S_{cr}) = 2.2$), there exist two solutions with different amplitudes (the so-called upper and

lower soliton branches). The sech-profiled solution given above describes only a portion of the lower soliton branch corresponding to the value of the parameter S that is much greater than the critical one.

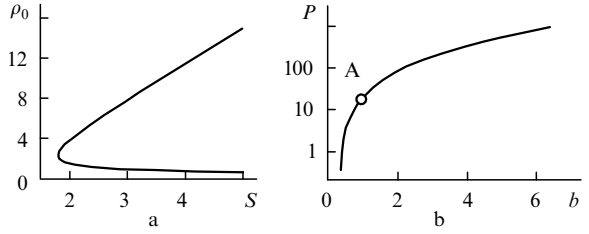

Figure 1. Dependences of the soliton amplitude ρ_0 on the parameter S (a) and of the soliton power on the propagation constant b (b). The point A divides the lower and upper soliton branches.

Note that already for $S > 3$ the amplitude of upper-branch solitons depends almost linearly on S, while the amplitude of lower-branch solitons is proportional to $S^{-1/2}$. The envelopes of the lower- and upper-branch solitons for $S = 1.9$ and 2.5 are shown in Fig. 2. These soliton profiles differ substantially from $\operatorname{sech}\eta$: the width of an exact soliton solution profile is smaller than the width of a sech-soliton with the same energy. Nevertheless, for small parameter values $S \sim 2 - 3$, an approximation of the form $\rho_0 \operatorname{sech}^m(q\eta)$ (where $m > 1$ for upper-branch solitons, $m < 1$ for lower-branch solitons, and the parameter q describes the soliton width) can be safely used.

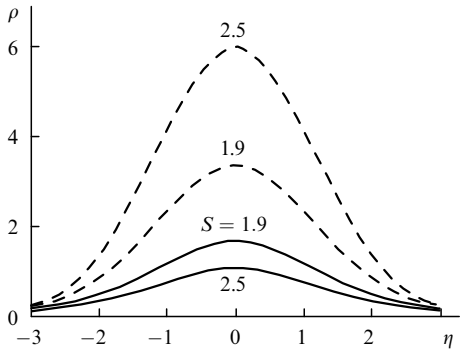

Figure 2. Profiles of the soliton-like beams belonging to the lower (the solid curves) and upper (the dashed curves) soliton branches for $S = 1.9$ and 2.5.

The stability of the above soliton solutions to small perturbations of the initial profile is confirmed by the well-known stability criterion stating that the solution is stable if the derivative $\partial P(b)/\partial b > 0$, where $P(b)$ is the beam power [21 – 23]. Employing expression (10) for the propagation constant and the results of numerical integration of the integral equation (9), we can verify that the power P of the soliton beam is a monotonically increasing function of the propagation parameter b for all $S \geqslant S_{cr}$ (see Fig. 1b). This means that the condition $\partial P(b)/\partial b > 0$ is fulfilled within the entire region of the existence of soliton solutions, which points to the stability of both lower- and upper-branch solitons. This theoretical statement was verified with the aid of numerical integration, which also indicated that the solitons of both branches were stable to significant (up to 10 % in intensity) harmonic and noise perturbations of the input profiles.

The studies of specific features of the interaction of intense light beams in the plasma medium under consideration are also of immediate practical interest. We analysed the interaction and collisions of soliton-like beams by numerically integrating Eqn (3) using the technique of decomposition in the physical factors. The initial conditions at the entrance to the plasma were specified in the following form:

$$\boldsymbol{a}_s(\eta, \xi = 0) = \boldsymbol{e}\rho(\eta + \eta_0)\exp[-i\alpha(\eta + \eta_0) + i\varphi] + \boldsymbol{e}\rho(\eta - \eta_0)\exp[i\alpha(\eta - \eta_0)]. \quad (11)$$

Here, η_0 is the initial distance between the centres of the beams, α is the angle of their convergence, and φ is the relative phase difference. Subsequently, the amplitudes of soliton-like beams were determined by numerical integration for a selected value of the parameter S and exact profiles were found employing the iterative procedure described above.

The collision dynamics of the soliton-like beams belonging to the upper soliton branch is given in Fig. 3 for different angles α and relative phase differences φ. Note that for the sake of convenience we can take as the initial soliton profiles not the exact profiles obtained numerically through the iterative procedure but approximate profiles described by the function $\rho(\eta) = \rho_0 \operatorname{sech}^m(q\eta)$, which adequately approximates the exact solution (for instance, for $S = 2.5$ and the upper-branch soliton, $\rho_0 = 5.98$, $m = 1.12$, and $q = 0.96$). The use of this approximation permits avoiding a number of numerical operations and virtually does not distort the collision dynamics, manifesting itself only in the weak scattering of excess energy during propagation of the beams.

As in the case of a Kerr medium, two in-phase ($\varphi = 0$) soliton-like beams launched parallel to each other ($\alpha = 0$) are mutually attracted. As the relative phase difference is increased from zero to π, the attraction gradually becomes weaker and then is replaced with repulsion. For small intersection angles $\alpha < 0.2$, two in-phase soliton-like beams may merge upon their interaction, forming a specific bound state (Fig. 3a). In this case, during propagation the in-phase beams periodically come together, intersect, and become separated by a certain distance. The maximum distance that separates the beams after their intersection decreases with decreasing the intersection angle α and the initial separation η_0 between the beams; in the limit for $\alpha \to 0$ and $\eta_0 \to 0$, a complete merging of the solitons can be attained.

The out-of-phase solitons cannot form a bound state, because this is hindered by their mutual repulsion. As the intersection angle increases, new beams can appear because of the interaction (to be more precise, the fraction of energy of the interacting beams imparted to the generated beams rises significantly with increasing angle α). Fig. 3b, for instance, depicts the generation of the third beam in the intersection of two in-phase soliton-like beams at an angle of $\alpha = 1.0$. Because of the energy transfer from the two parent beams to the generated beam, the former two lose their soliton properties; however, they do not spread out but propagate experiencing quasi-periodic oscillations. With an increase in the energy of the colliding solitons, i.e., in a medium with large S, the number of solitons generated at the same intersection angles increases.

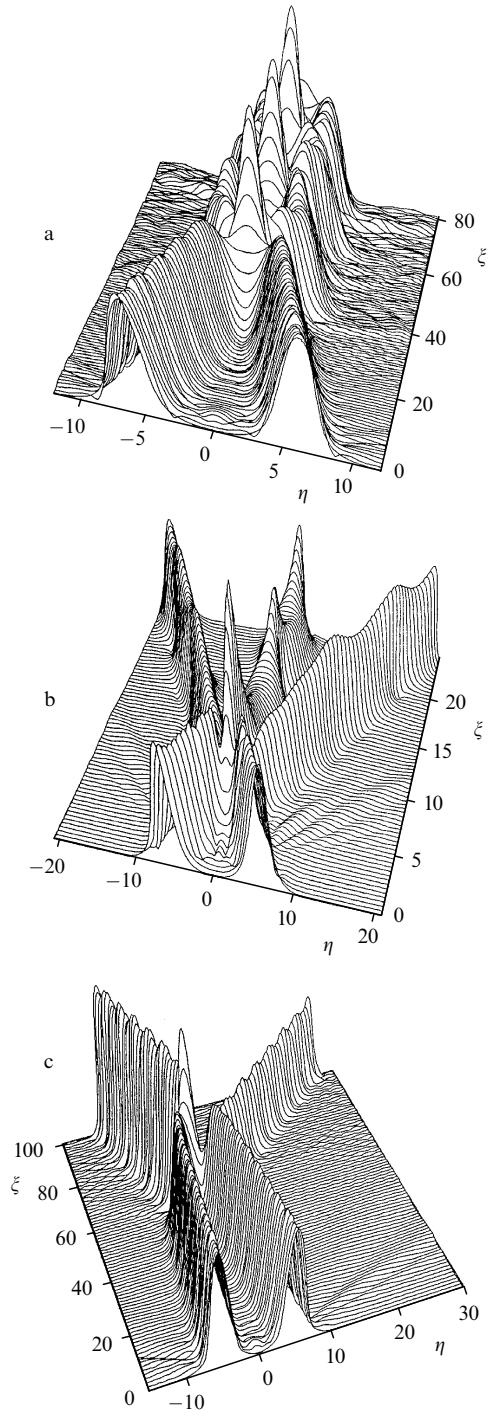

Figure 3. Dynamics of the collision of soliton-like beams belonging to the upper soliton branch in a medium with $S = 2.5$ for an intersection angle $\alpha = 0.1$ (a), 1.0 (b), and 0.04 (c) and a relative phase difference $\varphi = 0$ (a, b) and $\pi/4$ (c).

Collisions of antiphase beams can also result in the generation of new beams; however, this is possible only when the intersection angles are much higher than those in the in-phase case. When the relative phase difference φ of the intersecting beams is intermediate between zero and π, the inelastic energy transfer becomes quite significant, which results in the amplitude asymmetry of the beams that have experienced the interaction. The asymmetry of collision products is most pronounced for small angles α. Fig. 3c shows the intersection of two beams, which belong to the upper soliton branch, for $\alpha = 0.04$ and $\varphi = \pi/4$. One can see the distinct difference in both the amplitudes of the emergent beams and their propagation angles. All the above features of the interaction of soliton-like beams in a plasma with saturation also take place for the beams of the lower soliton branch.

4. Modulation instability of a plane wave

In this Section, we will consider the modulation instability of a plane wave in a fully ionised two-dimensional cold plasma using the truncated wave equation (3). The stationary solution of Eqn (3) that corresponds to a continuous wave with a constant amplitude has the form:

$$\boldsymbol{a}_s = \boldsymbol{e}\rho_0 \exp\left\{iS\xi\left[1 - \frac{1}{(1+\rho_0^2)^{1/2}}\right]\right\}. \tag{12}$$

A plane-wave model can be employed, for example, to describe the time evolution of small perturbations of the profile of a high-power laser beam when the beam radius greatly exceeds the characteristic perturbation scale. To investigate the modulation instability of a plane wave, we introduce a small perturbation in the initial field distribution:

$$\boldsymbol{a}_s = \boldsymbol{e}[\rho_0 + \delta\rho(\eta,\xi)] \exp\left\{iS\xi\left[1 - \frac{1}{(1+\rho_0^2)^{1/2}}\right]\right\}, \tag{13}$$

where $\delta\rho(\eta, \xi) \ll \rho_0$ is the slowly varying envelope of the modulation of the plane wave. By using a conventional linearisation technique and assuming that the amplitude of the initial harmonic perturbation varies according to the law $\delta\rho(\eta, \xi) \sim \exp(ig\xi - i\Omega\eta)$ during propagation, where g and Ω are the dimensionless wave number and spatial modulation frequency, we can obtain from Eqn (3) that for the frequencies Ω lying in the range from 0 to $(2S)^{1/2}\rho_0 \times(1+\rho_0^2)^{-3/4}$, the amplitude of a small perturbation during propagation will increase exponentially with the increment

$$G = \mathrm{Im}g = \frac{1}{2}\mathrm{Im}\left\{\Omega^2\left[\Omega^2 - \frac{2S\rho_0^2}{(1+\rho_0^2)^{3/2}}\right]\right\}^{1/2}. \tag{14}$$

The dependences of the increment G on the dimensionless spatial modulation frequency Ω for different amplitudes ρ_0 of the plane wave are given in Fig. 4. The increment attains a maximum at the frequency $\Omega_{max} = S^{1/2}\rho_0(1+\rho_0^2)^{-3/4}$. Because of the saturation of the nonlinear response, the modulation instability range narrows when the amplitude of the plane wave exceeds a certain value. For a fixed value of S, the maximum width of the modulation instability range is attained for $\rho_0 = 2^{1/2}$ and amounts to $2S^{1/2}/3^{3/4}$. If the modulation frequency lies outside the modulation instability range, no exponential perturbation occurs and harmonic oscillations of the perturbation amplitude with a period $2\pi/g$ arise.

The linearisation technique exactly predicts the boundaries of the modulation instability range but does not enable considering the mode of a developed instability. The most popular technique of investigating this mode, which involves the approximation of a finite (up to 5) number of harmonics in the emission spectrum, can be applied for a medium with saturation only in a narrow range of modulation frequencies Ω adjacent to the upper boundary of the modulation instability region. We will analyse the developed instability mode on

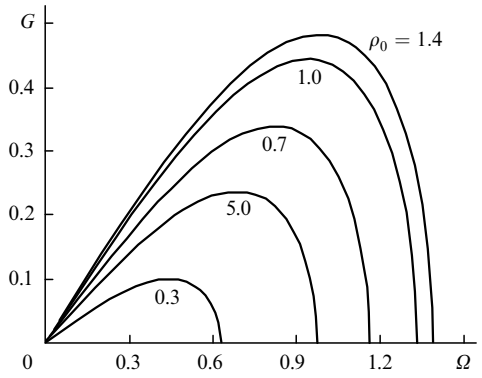

Figure 4. Dependences of the increment G on the dimensionless spatial modulation frequency Ω for different amplitudes of the plane wave for $S = 2.5$.

the basis of numerical simulations, nevertheless invoking the spectral criterion to determine the instability development length.

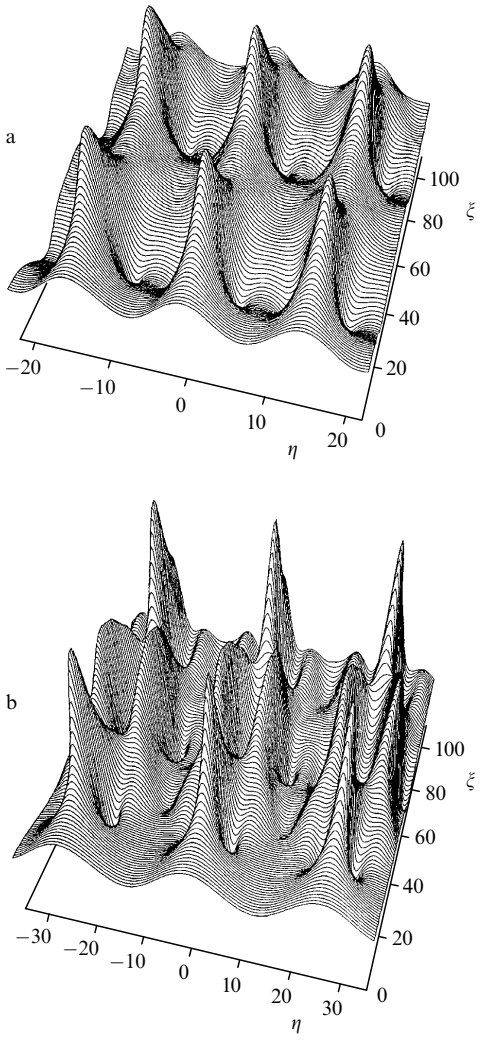

Figure 5. Dynamics of the development of a small ($\delta\rho = 0.05$) harmonic perturbation of a plane wave with the amplitude $\rho_0 = 0.3$ for $S = 2.5$ and modulation frequencies $\Omega_1 = 0.45$ (a) and $\Omega_2 = 0.3$ (b).

Fig. 5 shows the dynamics of the development of a small ($\delta\rho = 0.05$) harmonic perturbation of a plane wave with the amplitude $\rho_0 = 0.3$ for the modulation frequencies $\Omega_1 = \Omega_{\max} = 0.45$ and $\Omega_2 = (2/3)\Omega_{\max} = 0.3$ corresponding to the maximum increment. The initial exponential growth of the perturbation amplitude (broadly speaking, the growth law is described by the hyperbolic cosine), which leads to the filamentation of the plane wave into several localised beams (filaments), is followed by the reverse energy transfer to the plane wave (the zero harmonic).

This energy transfer may even result in the reconstruction of the initial profile of the perturbed plane wave (Fig. 5a). The dynamics of modulation instability development is more complicated at lower frequencies Ω (Fig. 5b). This is related to the fact that the spatial modulation period is in fact proportional to the energy that participates in the formation of a filament or a group of filaments and increases with lowering Ω as $2\pi/\Omega$. As a consequence, the number of filaments to which the plane wave decomposes increases significantly as the frequency Ω is lowered (Fig. 5b).

The dynamics of instability development, which is rather complicated in the time domain, allows a simple interpretation in the spectral domain. In spectroscopic terms, a filamentation means the energy transfer from the zero harmonic (a plane wave) to two harmonics at frequencies $\pm\Omega$ (which represent harmonic modulation) and the generation of new harmonics at multiple frequencies. In this connection the length of modulation instability development in the developed mode can be conveniently defined as the length L that corresponds to the maximum energy transfer from the zero harmonic (the plane wave) to the harmonics that are multiples of the frequency Ω. As the frequency Ω is reduced, the number of harmonics generated during propagation and the fraction of energy transferred from the zero harmonic increase significantly. In particular, the situation depicted in Fig. 5a corresponds to the excitation of four side harmonics at frequencies $\pm\Omega$ and $\pm 2\Omega$ and to a 45% energy transfer from the zero harmonic. The situation in Fig. 5b corresponds to the excitation of as many as eight harmonics and the 80% energy transfer.

Fig.6 shows the length L of modulation instability development as a function of the dimensionless modulation frequency Ω for several values of the plane-wave amplitude. Note that the frequency obtained by numerical integration, which corresponds to the fastest instability development, coincides with the frequency $\Omega_{\max} = S^{1/2}\rho_0/(1+\rho_0^2)^{3/4}$ predicted using the linearisation technique. Interestingly, the closer the amplitude of a plane wave to the amplitude $\rho_0 = 2^{1/2}$ cor-

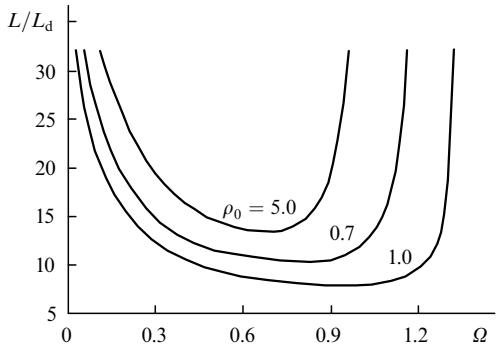

Figure 6. Length L of modulation instability development as a function of the dimensionless modulation frequency Ω for several amplitudes of the plane wave for $S = 2.5$.

responding to the maximum width of the instability range, the broader the modulation frequency range in which the length of instability development is nearly constant. This is substantially different from the function (14). As the modulation frequency approaches the boundary of the instability region, the length L of instability development tends to infinity.

Apart from the modulation frequency, the length of instability development depends substantially on the ratio between the amplitudes of the start-up perturbation and of the plane wave. Fig. 7 shows the dependence of L on this ratio $\delta\rho/\rho_0$ for the frequency $\Omega_{\max}$ corresponding to the fastest instability development. It is evident that L exhibits, as in the previous case, a weak dependence on the $\delta\rho/\rho_0$ ratio when the amplitude of the plane wave approaches the value $\rho_0 = 2^{1/2}$, which corresponds to the maximum width of the instability range.

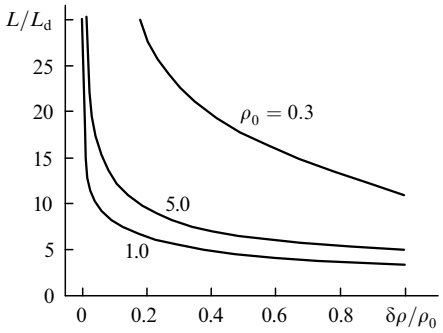

Figure 7. Length L of modulation instability development as a function of the ratio $\delta\rho/\rho_0$ between the start-up perturbation and plane-wave amplitudes for the frequency $\Omega_{\max}$ corresponding to the largest instability increment G, and $S = 2.5$.

References

1. Borghesi M, MacKinnon A, Barringer L, Gaillard R, Gizzi L, Meyer C, Willi O, Pukhov A, Meyer-ter-Vehn J *Phys. Rev. Lett.* **78** 879 (1997)
2. Krushelnick K, Ting A, Moore C, Burris H, Erasey E, Sprangle P, Baine M *Phys. Rev. Lett.* **78** 4047 (1997)
3. Fuchs J, Malka G, Adam J, Amiranoff F, Baton S, Blanchot N, Heron A, Laval G, Miquel J, Mora P, Pepin H, Rousseaux C *Phys. Rev. Lett.* **80** 1658 (1998)
4. Hamster H, Sullivan A, Gordon S, White W, Falcone R *Phys. Rev. Lett.* **71** 2725 (1993)
5. Sprangle P, Erasey E, Ting A, Joyce G *Appl. Phys. Lett.* **53** 2146 (1988)
6. Tsytovich V, DeAngelis U, Bingham R *Comments Plasma Phys. Controlled Fusion* **12** 249 (1989)
7. Shkolnikov P, Kaplan A, Pukhov A, Meyer-ter-Vehn J *Appl. Phys. Lett.* **71** 3471 (1997)
8. Wagner R, Chen S, Maksimchuk A, Umstadter D*Phys. Rev. Lett.* **78** 3125 (1997)
9. Moore C, Ting A, Krushelnick K, Erasey E, Hubbard R, Hafizi B, Burris H, Manka C, Sprangle P *Phys. Rev. Lett.* **79** 3909 (1997)
10. Malka G, Miquel J *Phys. Rev. Lett.* **77** 75 (1996)
11. Erasey E, Hubbard R, Leemans W, Ting A, Sprangle P *Phys. Rev. Lett.* **79** 2682 (1997)
12. Pukhov A, Meyer-ter-Vehn J *Phys. Rev. Lett.* **76** 3975 (1996)
13. Malka G, Fuchs J, Amiranoff F, Baton S, Gaillard R, Miquel J, Pepin H, Rousseaux C, Bonnaud G, Busquet M, Lours L *Phys. Rev. Lett.* **79** 2053 (1997)
14. Antonsen T, Mora P *Phys. Rev. Lett.* **69** 2204 (1992)
15. Sprangle P, Erasey E, Krall J, Joyce G *Phys. Rev. Lett.* **69** 2200 (1992)
16. Sprangle P, Erasey E, Ting A *Phys. Rev. A* **41** 4463 (1990)
17. Sprangle P, Erasey E, Hafizi B *Phys. Rev. Lett.* **79** 1046 (1997)
18. Noble R *Phys. Rev. A* **32** 460 (1985)
19. Gatz S, Hermann J *J. Opt. Soc. Am. B: Opt. Phys.* **8** 2296 (1991)
20. Gatz S, Hermann J *J. Opt. Soc. Am. B: Opt. Phys.* **14** 1795 (1997)
21. Vakhitov N G, Kolokolov A A *Izv. Vyssh. Uchebn. Zaved. Ser. Radiofiz.* **16** 1020 (1973)
22. Mitchell D, Snyder A *J. Opt. Soc. Am. B: Opt. Phys.* **10** 1572 (1993)
23. Tran H *J. Opt. Soc. Am. B: Opt. Phys.* **11** 789 (1994)